Gao et al. Nanoscale Research Letters (2016) 11:463
DOI 10.1186/s11671-016-1677-1

Nanoscale Research Letters

NANO EXPRESS Open Access

Enhancing Performance of CdS Quantum Dot-Sensitized Solar Cells by Two-Dimensional g-C_3N_4 Modified TiO_2 Nanorods

Qiqian Gao, Shihan Sun, Xuesong Li*, Xueyu Zhang, Lianfeng Duan and Wei Lü*

Abstract

In present work, two-dimensional g-C_3N_4 was used to modify TiO_2 nanorod array photoanodes for CdS quantum dot-sensitized solar cells (QDSSCs), and the improved cell performances were reported. Single crystal TiO_2 nanorods are prepared by hydrothermal method on transparent conductive glass and spin-coated with g-C_3N_4. CdS quantum dots were deposited on the g-C_3N_4 modified TiO_2 photoanodes via successive ionic layer adsorption and reaction method. Compared with pure TiO_2 nanorod array photoanodes, the g-C_3N_4 modified photoanodes showed an obvious improvement in cell performances, and a champion efficiency of 2.31 % with open circuit voltage of 0.66 V, short circuit current density of 7.13 mA/cm^2, and fill factor (FF) of 0.49 was achieved, giving 23 % enhancement in cell efficiency. The improved performances were due to the matching conduction bands and valence bands of g-C_3N_4 and TiO_2, which greatly enhanced the separation and transfer of the photogenerated electrons and holes and effectively suppressed interfacial recombination. Present work provides a new direction for improving performance of QDSSCs.

Keywords: g-C_3N_4, TiO_2 nanorod arrays, Photoelectronical performance, Solar cells

Background

As one kind of novel solar cells, quantum dot-sensitized solar cells (QDSSCs) have attracted worldwide scientific and technological interest [1]. Basically, the structure of a QDSSC includes photoanode (a layer of porous oxide semiconductor with wide bandgap covered by semiconductor QDs as sensitizers), liquid electrolyte, and counter electrode. Many factors such as morphologies of oxide semiconductors, selection of sensitizers, and counter electrodes et al. could greatly affect the photoelectric conversion efficiency (PCE) of QDSSCs. Therefore, many efforts have been devoted to investigate these factors. Recently, a PCE of 9.01 % was achieved using $CdSe_{0.65}Te_{0.35}$ quantum dot (QD) as sensitizers [2]. However, the PCE of QDSSC is still far behind its theoretical efficiency, and further researches from different aspects are still required to improve the efficiencies of QDSSCs.

TiO_2 is one of the most important semiconductors as the photoanode material which is the key components in the configuration of QDSSCs. Since the breakthrough work on colloidal TiO_2 based DSSCs by O'Regan and Grätzel in 1991, various TiO_2 nanostructures have been used in QDSSC, like nanoparticles, nanosheet, and nanorod [3–8]. Among them, single-crystalline TiO_2 nanorod array would be one of the most desirable nanostructures for preparing photoanode of QDSSC due to its effective charge transfer property as well as excellent light harvesting ability. Inorganic semiconductors QDs such as CdS, PbS, PbSe, CdTe, CdSe, and Bi_2S_3 have been used to assist as a sensitizer for solar devices [9]. Among them, CdS is considered to be one of the potential photovoltaic semiconductive materials for its broadly tunable bandgap. The combination of wide bandgap semiconductors and CdS QDs can preferably collect the visible light used in photoelectrochemical applications.

* Correspondence: lixuesong@ccut.edu.cn; lw771119@hotmail.com
Key Laboratory of Advanced Structural Materials, Ministry of Education, Changchun University of Technology, Changchun 130012, China

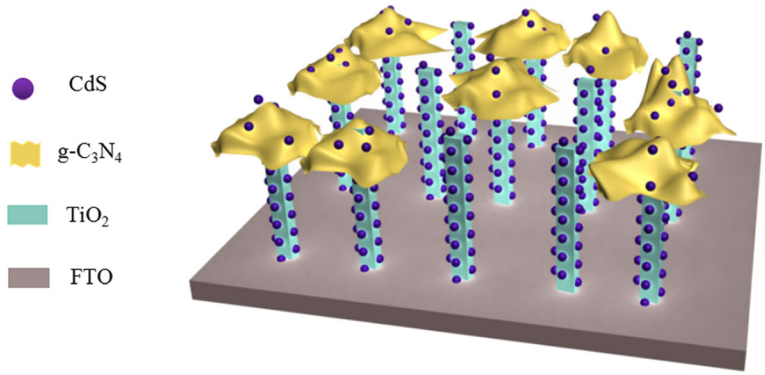

Scheme 1 Schematic illustration of CdS/g-C_3N_4/TiO_2 nanorod photoanode structure

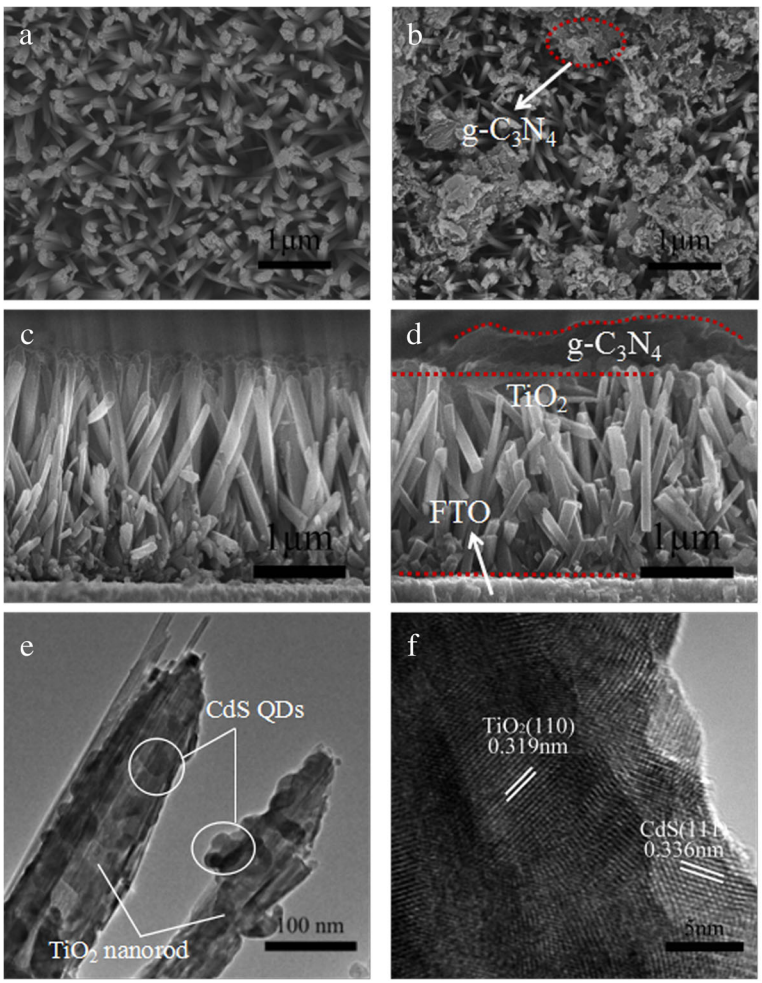

Fig. 1 Morphologies of TiO_2/FTO and g-C_3N_4/TiO_2/FTO photoelectrodes: typical top view SEM images of TiO_2/FTO photoelectrode (**a**) and g-C_3N_4/TiO_2/FTO photoelectrode (**b**); typical cross-sectional view of the well-aligned TiO_2 nanorod array (**c**) and g-C_3N_4/TiO_2 photoelectrode (**d**); typical TEM image of single TiO_2 nanorod deposited with CdS QDs (10 cycles) (**e**), and HRTEM of CdS QD decorated TiO_2 nanorod (**f**)

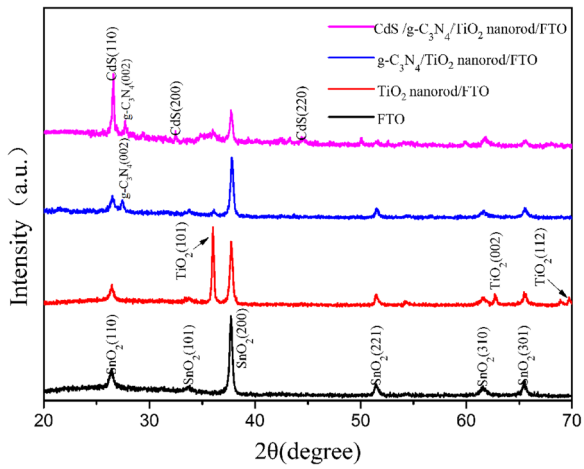

Fig. 2 The XRD patterns for FTO substrate, TiO_2/FTO, g-C_3N_4/TiO_2/FTO, and CdS/g-C_3N_4/TiO_2/FTO

One of obstacles which limit the performance of QDSSCs is the photogenerated carrier recombination. In order to restrain such recombination, introducing a passivation layer such as Al_2O_3 and ZnS between photoanode and electrolyte would be an effective method [10], which can retard the recombination by partially separating the electrons and electrolyte. Recently, graphitic carbon nitride (g-C_3N_4) has drawn much attention as a metal-free photocatalyst due to high photocatalytic efficiency.[11–13] Due to the band structure of g-C_3N_4, type II band alignment could be formed between g-C_3N_4 and TiO_2, which can significantly prevent the migration of photogenerated electrons from TiO_2 and QDs to the electrolyte [14]. Moreover, introducing g-C_3N_4 could expand the absorption range of sunlight. Therefore, introducing g-C_3N_4 into TiO_2-based photoanodes should improve the performance of QDSSCs.

However, most reports about applications of g-C_3N_4 are for photocatalysts, and few works for solar cells could be found. Very recently, Wu et al. reported the improved short circuit current of ZnO-based dye-sensitized solar cells (DSSCs) using g-C_3N_4 as multifunctional protecting layer of ZnO particles [15]. Xu et al. reported enhanced PCE of DSSCs using g-C_3N_4 modified TiO_2 nanosheets [16]. In present work, we investigated the effect of g-C_3N_4 as both recombination retarding layer and sensitizer on the performance of QDSSC. Single crystal TiO_2 nanorod array was prepared by hydrothermal method on a transparent conducting glass and spin-coated with g-C_3N_4, leading to the formation of g-C_3N_4/TiO_2 heterostructure. Compared with pure TiO_2 nanorod array photoanodes, the g-C_3N_4 modified photoanodes showed an obvious improvement in cell performances. The results of I-V characteristic exhibited that introducing g-C_3N_4 increased both the open circuit voltage and short circuit photocurrent density, and the possible mechanism is discussed.

Methods

Materials

FTO glasses were purchased from Zhuhai Kaivo Optoelectronic Technology Co., Ltd. Acetone, ethanol, hydrochloric acid, and cadmium acetate and methanol were purchased from Beijing Chemical Works. Titanium butoxide was purchased from Shanghai Chemicals. Melamine, Na_2S, S, urea, and acetic acid were purchased from Aladdin. $CuSO_4$ was acquired from Tianjin Guangfu Technology Development Co., Ltd. $Na_2S_2O_3$ was purchased from Damao Chemical Reagent, Tianjin.

Preparation of TiO_2 Nanorod Arrays

TiO_2 nanorod array was fabricated according to the previous report [17]. Typically, 15 mL of deionized water was mixed with 15 mL hydrochloric acid. The mixture was then stirred for 15 min followed by the addition of 0.5 mL of titanium butoxide. The mixture was transferred into a 45-mL autoclave. Then, cleaned FTO substrates were put into the autoclave, and the hydrothermal process was conducted at 150 °C for 12 h.

Preparation of g-C_3N_4 Paste

The g-C_3N_4 was prepared using the method reported previously [18–20]. Briefly, 3 g melamine and 4 g urea were mixed in a 20-mL crucible, transferred into a muffle furnace, and heated to and kept at 550 °C for 2 h. The yellow crystalline g-C_3N_4 bulk was obtained and then fully grinded into pale yellow powders. The g-C_3N_4 paste was prepared by mixing g-C_3N_4 powders (0.8 g), ethyl cellulose (0.4 g), and α-terpinol (3.245 g) in anhydrous ethanol (8.5 mL) and stirring the mixture for 24 h.

Preparation of CdS/g-C_3N_4/TiO_2 Photoanodes

The g-C_3N_4 paste was spin-coated on the as-prepared TiO_2 nanorod. The as-received g-C_3N_4/TiO_2 nanorod photoanodes were subjected to a sintering process in air at 450 °C for 30 min. After cooling to room temperature, the photoanodes were decorated with CdS QDs by successive ionic layer adsorption and reaction (SILAR) method [21]. The g-C_3N_4/TiO_2 nanorod photoanode was successively dipped in a 0.05 M cadmium acetate methanol solution and a 0.05 M Na_2S methanol solution each for 30 s. The two-step dipping procedure was termed as one cycle. The illustration of photoanode structure is shown in Scheme 1.

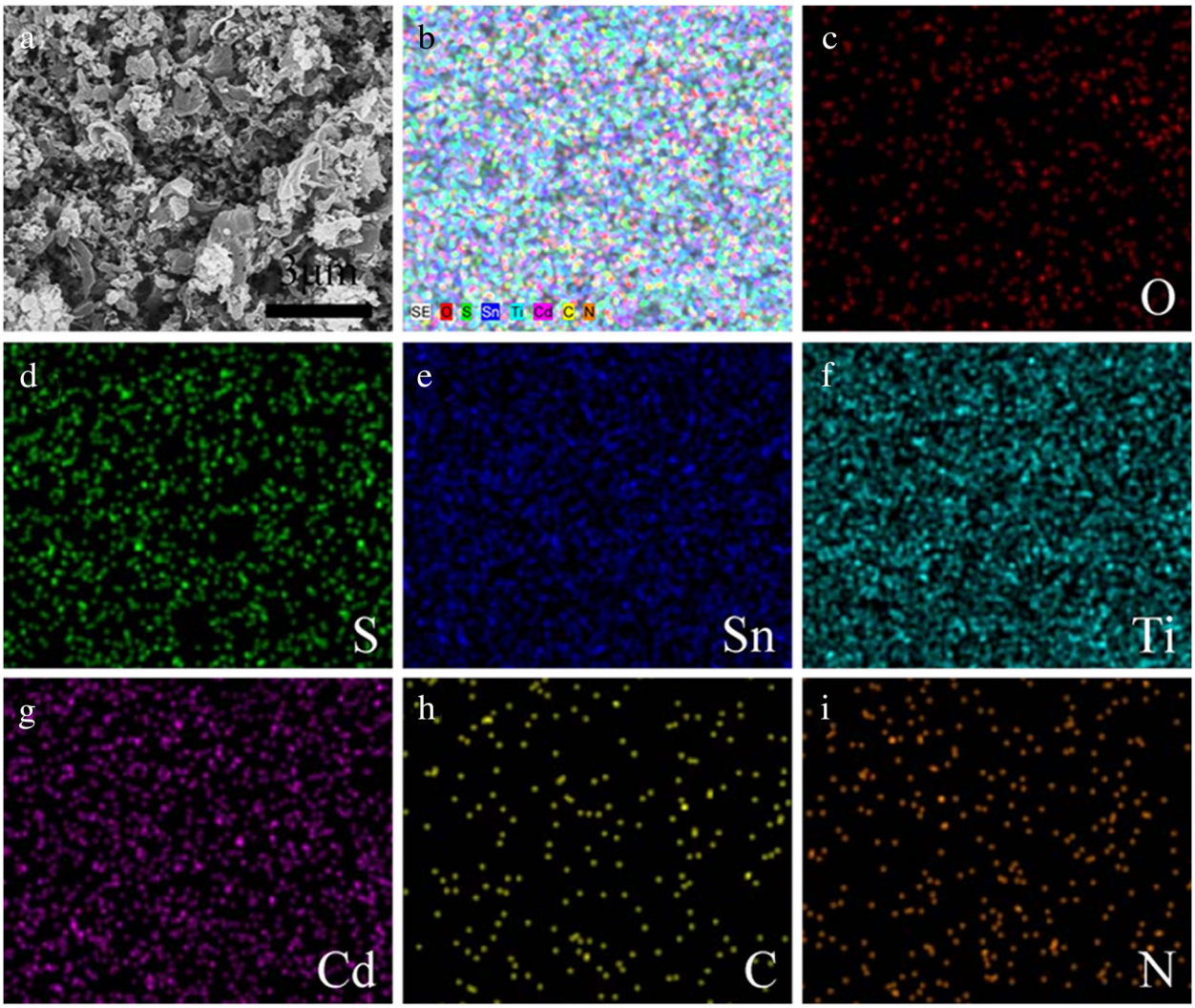

Fig. 3 The EDX mapping images of CdS/g-C_3N_4/TiO_2photoanode:SEM of CdS/g-C_3N_4/TiO_2(a);EDX mapping of O,S,Sn,Ti,Cd,C,N(b);Element mapping of O(c),S(d),Sn(e),Ti(f),Cd(g),C(h),N(i)

Preparation of CuS Counter Electrodes

CuS counter electrodes were made by chemical bath deposition (CBD) method. One molar $CuSO_4$ aqueous solution and 1 M $Na_2S_2O_3$ aqueous solution were mixed with the volume ratio of 1:4. The pH of the mixed solution was adjusted to 2 with acetic acid. Then, the FTO glasses were immersed into 100 mL as-prepared mixed solution. The above solution was heated to 70 °C and kept for 4 h. After cooling down to the room temperature, the substrates were washed and dried in air and then heated to 130 °C and kept for 30 min.

Fabrication of QDSSCs

The as-prepared CdS/g-C_3N_4/TiO_2 nanorod photoanode and CuS counter electrode were assembled to a sandwich-type cell and penetrated with a polysulde electrolyte that consisted of 1 M Na_2S and 1 M S in methanol and H_2O solution (v/v = 7:3).

Characterization

The samples were characterized using field emission scanning electron microscopy (FESEM, S4800, Hitachi), transmission electron microscopy (TEM) (Tecnai F20), X-ray diffraction (XRD) (D-MAX II A X-ray diffractmeter), X-ray photoelectron spectra (XPS) (VG ESCALAB MKII), and Fourier transform infrared spectroscopy (FTIR) (VERTEX 70). The cell performances were investigated by AM 1.5 solar simulator and Solar Cell Scan 100 (Zolix, Beijing).

Results and Discussion

The morphologies of the as-prepared TiO_2 nanorods and g-C_3N_4/TiO_2 nanorods on FTO substrate are shown

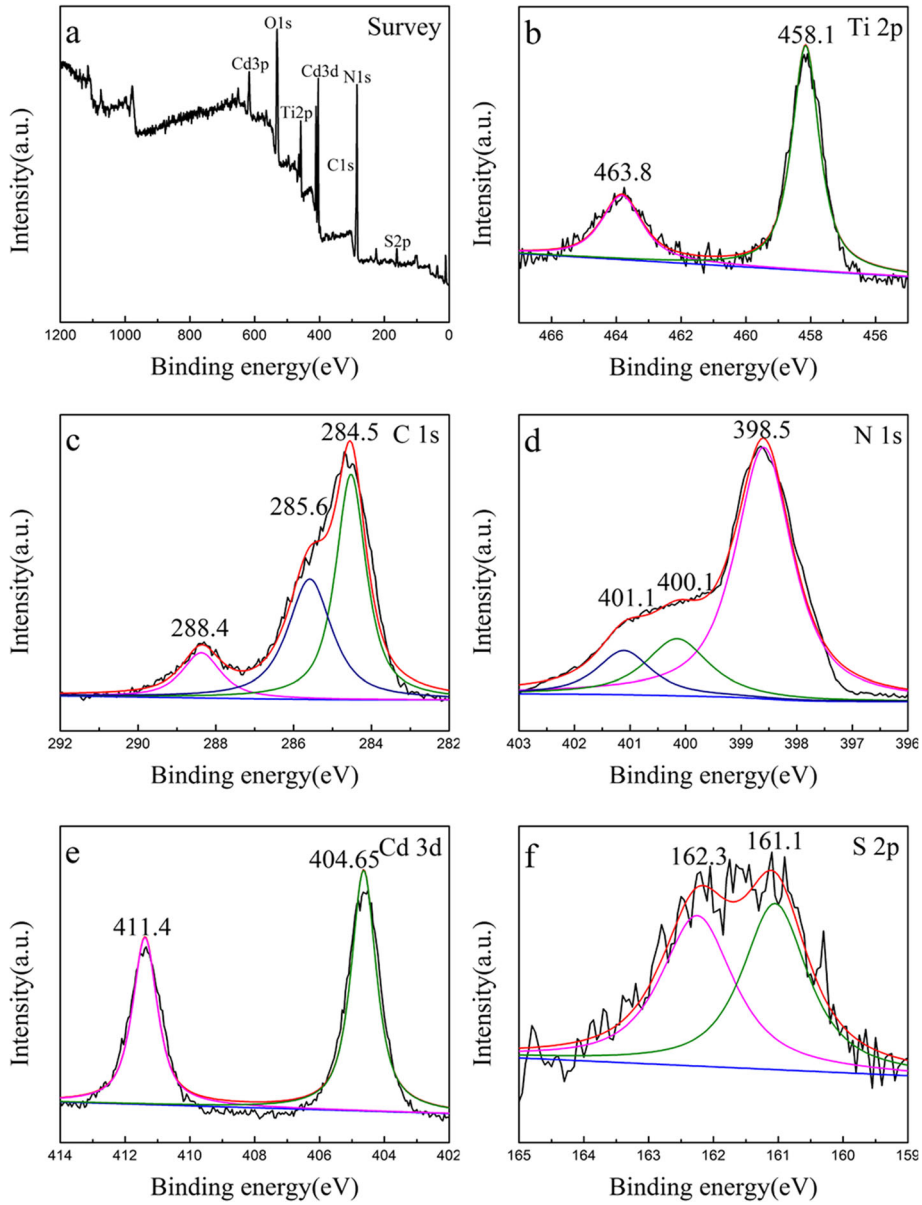

Fig. 4 XPS spectrum of the as-prepared photoanode **a** survey, **b** Ti1s, **c** C1s, **d** N1s, **e** Cd 3d, and **f** S 2p

in Fig. 1. As shown in Fig. 1a, TiO_2 nanorods with high density in the average diameter ~100 nm are formed uniformly on FTO substrate. For these nanorods, while the side facets are smooth, the shape of top facets is square and composed of many step edges. These steps are responsible for further growth of the TiO_2 nanorod, and these results show the expected growth habit of the tetragonal crystal. From the cross-sectional image of the sample as shown in Fig. 1c, it is obvious that the well-aligned nanorods are nearly normal to the FTO substrate. The length of the nanorods is about 3 μm. For TiO_2 nanorods capped by g-C_3N_4, Fig. 1b shows that discontinuous g-C_3N_4 layer was coated on the surface of TiO_2 nanorods. These remaining vacancies could assure that CdS quantum dots can be deposited on g-C_3N_4 as well as TiO_2 nanorods. The cross-sectional view in Fig. 1d indicates that g-C_3N_4 was successfully coated on the TiO_2 nanorods with the thickness of about 0.8 μm. Figure 1e shows the TEM image of TiO_2 nanorod decorated with CdS QDs for 10 cycles. Compared with bare TiO_2 nanorod, the rough surface could be observed after CdS QD deposition, indicating that large amounts of

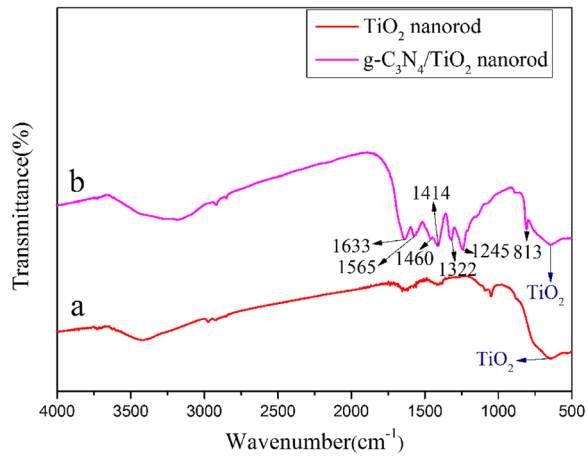

Fig. 5 FTIR spectrum of bare TiO_2 nanorod and g-C_3N_4/TiO_2 nanorod

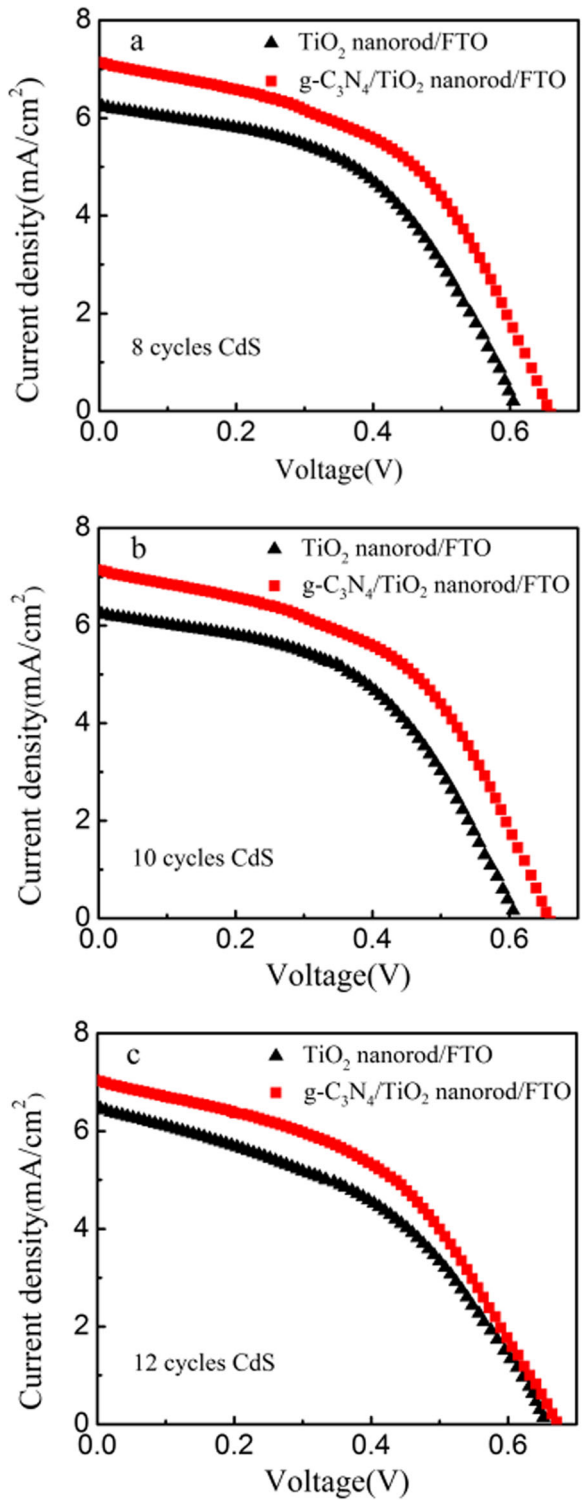

Fig. 6 I-V curves acquired using CdS/TiO_2 and CdS/g-C_3N_4/TiO_2 photoanodes with different CdS QD SILAR cycles: 8 cycles (**a**), 10 cycles (**b**), and 12 cycles (**c**)

CdS QDs had been deposited on the TiO_2 nanorods. This is further confirmed by HRTEM image (Fig. 1f). The lattice fringe space of 0.319 and 0.336 nm corresponds to the (110) plane of tetragonal rutile TiO_2, and (111) planes of the cubic phase of CdS could be confirmed.

Figure 2 shows the XRD curves of FTO substrate, TiO_2/FTO, g-C_3N_4/TiO_2/FTO, and CdS/g-C_3N_4/TiO_2/FTO, respectively. The XRD result of TiO_2/FTO exhibits a greatly increased (002) and (101) diffraction, suggesting the vertical growth of highly oriented titania nanorods on FTO, which is consistent with SEM observation. After coating with g-C_3N_4, a peak at 27.7° could be observed which is attributed to the typical (002) plane of the g-C_3N_4. After the deposition of CdS QDs, the XRD pattern of CdS/g-C_3N_4/TiO_2/FTO shows diffraction peaks corresponding to the hexagonal wurtzite phase of CdS. Figure 3 shows the EDX mapping images of CdS/g-C_3N_4/TiO_2 photoanode. The Sn comes from FTO substrate, and O is originated from FTO substrate and TiO_2 nanorods. The same position of S and Cd indicates the CdS QD formation. The position distribution of C and N is similar, indicating the formation of g-C_3N_4 after spin coating. The EDX results are further confirmed by XPS.

The XPS survey in Fig. 4a exhibits that the existence of C, N, Cd, S, Ti, and O in the CdS/g-C_3N_4/TiO_2 photoanode. The Ti 2p3/2 and 2p1/2 centered at 458.1 and 463.8 eV are in agreement with those of pure TiO_2 (Fig. 4b) [22–25]. The C 1s shown in Fig. 3c has three peaks situated at 284.5, 288.4, and 285.6 eV, which corresponds to sp2 C–C bonds, sp2-bonded carbon in N–C=N, and sp3-bonded carbon species, respectively. For N, three peak signals of N1s located at 398.5, 400.1, and

Table 1 Photovoltaic performance parameters of CdS/TiO_2 and $CdS/g\text{-}C_3N_4/TiO_2$ electrodes

Samples	Cycles	Jsc (mA/cm^2)	Voc (V)	FF	η (%)
TiO_2 nanorod	8	5.86	0.56	0.51	1.67
	10	6.25	0.61	0.50	1.88
	12	6.48	0.65	0.43	1.83
TiO_2 nanorod/g-C_3N_4	8	6.85	0.65	0.47	2.11
	10	7.13	0.66	0.49	2.31
	12	7.03	0.67	0.47	2.21

401.1 eV are present and attributed to sp2 bond N in triazine rings, tertiary N in N-(C)3 units, respectively [26]. These results indicate the presence of graphite-like C_3N_4. Moreover, the Cd 3d-related peaks at 404.65 and 411.4 eV are observed and attributed to Cd 3d5/2 and Cd 3d3/2, respectively. The S2p XPS spectra can be separated to two peaks at 161.1 and 162.3 eV which are ascribed to S^{2-} in CdS [27].

Figure 5 shows the comparison of the FTIR spectra of pure TiO_2 nanorod and TiO_2 nanorod/g-C_3N_4. The strong absorption between 500 to 800 cm^{-1} represents the bonds of Ti–O–Ti in both of the curves [28]. When g-C_3N_4 sheets are coated on TiO_2 nanorods, several strong bands could be observed in the range of 1200–1700 cm^{-1} which are typical stretching modes of CN heterocycles [29]. Moreover, the peak at 813 cm^{-1} is due to variation of triazine units [30]. These absorption peaks once again confirm the existence of C_3N_4 on the as-prepared TiO_2 nanorod photoanode.

The cell performances are investigated as shown Fig. 6, and corresponding parameters are listed in Table 1. For both CdS/TiO_2 and $CdS/g\text{-}C_3N_4/TiO_2$ electrodes, the cell performances with different deposition cycles of CdS QDs are investigated. Both two kinds of electrodes exhibit the best performance with 10 cycles of CdS QD deposition, and the efficiency decreases with further increasing deposition cycles. This is probably due to the excessive deposition of QDs. If the deposition cycles of CdS QDs are more than 10, CdS QD with larger average size would be produced, and the aggregation and convergence among CdS QDs could happen at the surface of g-C_3N_4/TiO_2. The larger CdS QDs would have poor ability to generate multiple excitons, originating from the disappearance of the quantum effect [31]. As shown in Table 1, the measurements of I-V characteristic indicate that the addition of g-C_3N_4 increases both the open circuit voltage and short circuit photocurrent density. As shown in Fig. 7, the photon-to-current conversion efficiency (IPCE) value is improved after coating g-C_3N_4 in the range of 300–600 nm. Compared with CdS/TiO_2 electrode, it is worth noticing that the IPCE of CdS/g-C_3N_4/TiO_2 electrodes is enhanced obviously between 400 and 500 nm. The maximum IPCE value occurs at ~470 nm which is very close to the bandgap of g-C_3N_4 used in this work. The improvement of IPCE could be due to the synergistic effect of g-C_3N_4 and CdS QD for sensitizing TiO_2 nanorods.

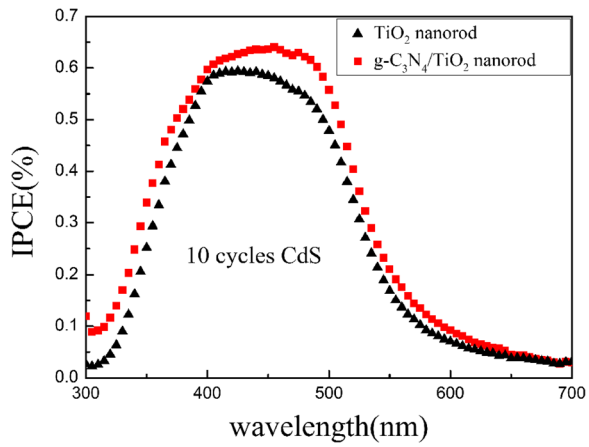

Fig. 7 IPCE of 10 cycles CdS/TiO_2 and 10 cycles $CdS/g\text{-}C_3N_4/TiO_2$ electrodes

The mechanism of the performance improvement of QDSSCs in this work is suggested as below. As illustrated in Fig. 8, a type II band alignment between TiO_2 and g-C_3N_4 could be built due to suitable band structure of g-C_3N_4. Therefore, the immigration of photogenerated electrons from the conduction band (CB) of TiO_2 and CdS QDs to g-C_3N_4 and electrolyte would be restrained. The g-C_3N_4 layer on TiO_2 nanorods acted as both block layer and effective light absorption layer could effectively promote the electron transport by retarding the backward recombination of electrons from TiO_2 and electrolyte and also contribute additional electrons to increase the electron concentration in the photoanodes, thus to enhance the performance of QDSSCs. Moreover, the synergistic effect of g-C_3N_4 and CdS QDs for sensitizing TiO_2 nanorods would be the other reason. As shown in IPCE measurement, introducing g-C_3N_4 will further improve photoelectron injection to TiO_2 particularly in the range of 400–500 nm, which suggests that the existence of g-C_3N_4 layer will supplement the adsorption of sunlight. The matching conduction bands and valence bands of g-C_3N_4 and TiO_2 greatly enhanced the separation and transfer of the photogenerated electrons and holes in the composite; thus, the photoelectrochemical performance of the g-C_3N_4/TiO_2 electrode is improved.

Conclusions

In summary, we introduce two-dimensional g-C_3N_4 layer in the single crystal TiO_2 nanorod array photoanode.

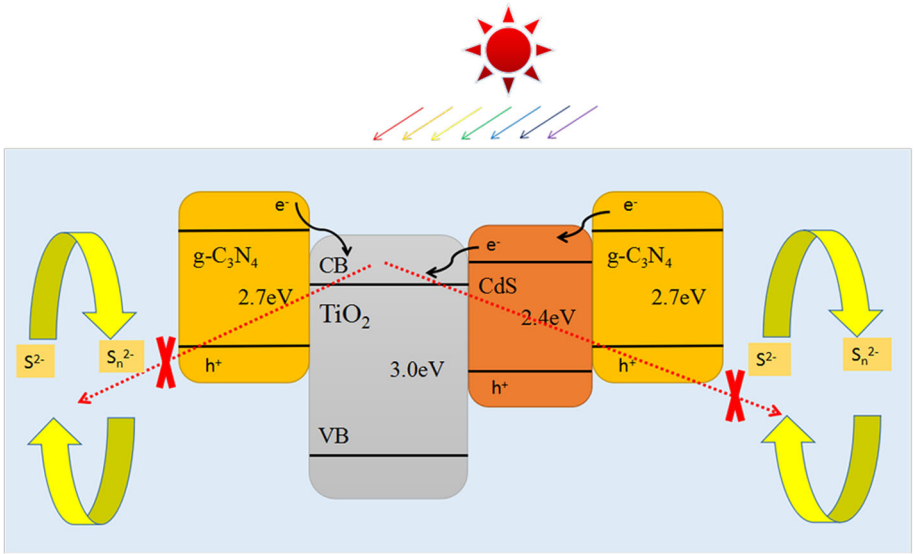

Fig. 8 Mechanism of charge separation and transfer between g-C_3N_4 and TiO_2 nanorod arrays under visible light irradiation

Compared with pure TiO_2 nanorod array photoanodes, the g-C_3N_4 modified photoanodes showed an obvious improvement in cell performances, and a champion efficiency of 2.31 % was achieved, giving 23 % enhancement in cell efficiency. The improved performances were due to the matching conduction bands and valence bands of g-C_3N_4 and TiO_2, which greatly enhanced the separation and transfer of the photogenerated electrons and holes and effectively suppressed interfacial recombination. Present work provides a new direction for improving the performance of QDSSCs.

Abbreviations

CBD: Chemical bath deposition; DSSCs: Dye-sensitized solar cells; FESEM: Field emission scanning electron microscopy; FF: Fill factor; g-C_3N_4: Graphite carbon nitride; QDs: Quantum dots; QDSSCs: Quantum dot-sensitized solar cells; SILAR: Successive ionic layer adsorption and reaction; TEM: Transmission electron microscopy; XPS: X-ray photoelectron spectra

Acknowledgements

Financial support from the National Natural Science Foundation of China (authorization numbers: 61376020, 61574021) and the Science and Technology Department of Jilin Province (20130101009JC, 20140414024GH) is acknowledged.

Authors' Contributions

WL and XL conceived the idea. QG carried out the experiments. SS, XZ, and LD took part in the experiments and the discussion of the results. WL, QG, and XL drafted the manuscript. All authors read and approved the final manuscript.

Competing Interests

The authors declare that they have no competing interests.

Received: 9 September 2016 Accepted: 5 October 2016
Published online: 18 October 2016

References

1. Chuang CM, Brown PR, Bulovic V, Bawendi MG (2014) Improved performance and stability in quantum dot solar cells through band alignment engineering. Nat Mater 13:796
2. Ren Z, Wang J, Pan Z, Zhao K, Zhang H, Li Y et al (2015) Amorphous TiO_2 buffer layer boosts efficiency of quantum dot sensitized solar cells to over 9%. Chem Mater 27:8398
3. Weng ZY, Guo H, Liu XM, Wu SL, Yeung KW, Chu PK (2013) Nanostructured TiO_2 for energy conversion and storage. RSC Adv 3:24758
4. Chen X, Jia B, Zhang Y, Gu M (2013) Exceeding the limit of plasmonic light trapping in textured screen-printed solar cells using Al nanoparticles and wrinkle-like graphene sheets. Light-Sci Appl 2:e92
5. Jiu JT, Isoda S, Wang FM, Adachi M (2006) Dye-sensitized solar cells based on a single-crystalline TiO_2 nanorod film. J Phys Chem B 110:2087
6. Song MY, Ahn YR, Jo SM, Kim DY, Ahn J (2005) TiO_2 single-crystalline nanorod electrode for quasi-solid-state dye-sensitized solar cells. Appl Phys Lett 87:113113
7. Zhang XY, Sun SH, Sun XJ, Zhao YR, Chen L, Yang Y (2016) Plasma-induced, nitrogen-doped graphene-based aerogels for high-performance supercapacitors. Light-Sci Appl 5:e16130
8. Wang H, Bai YS, Zhang H, Zhang ZH, Li JH, Guo L (2010) CdS quantum dots-sensitized TiO_2 nanorod array on transparent conductive glass photoelectrodes. J Phys Chem C 114:16451
9. Bhande SS, Ambade RB, Shinde DV, Ambade SB, Patil SA, Naushad M et al (2015) Improved photoelectrochemical cell performance of tin oxide with functionalized-multiwalled carbon nanotubes-cadmium selenide sensitizer. ACS Appl Mater Interface 7:25094
10. Lee YL, Lo YS (2015) Highly efficient quantum-dot-sensitized solar cell based on co-sensitization of CdS/CdSe. Adv Funct Mater 19:604
11. Ayan-Varela M, Villar-Rodil S, Paredes JI, Munuera JM, Pagán A, Lozano-Pérez AA et al (2015) Investigating the dispersion behavior in solvents, biocompatibility, and use as support for highly efficient metal catalysts of exfoliated graphitic carbon nitride. ACS Appl Mater Interface 7:24032
12. Wang XC, Maeda K, Thomas A, Takanabe K, Xin G, Carlsson JM et al (2009) A metal-free polymeric photocatalyst for hydrogen production from water under visible light. Nat Mater 8:76
13. Chen HM, Xie YH, Sun XQ, Lv ML, Wu FF, Zhang L et al (2015) Efficient charge separation based on type-II g-C_3N_4/TiO_2-B nanowire/tubes heterostructure photocatalysts. Dalton Trans 44:13030
14. Low JX, Cao SW, Yu JF, Wageh S (2014) Two-dimensional layered composite photocatalysts. Chem Commun 50:10768
15. Wu DP, Cao K, Wang FJ, Wang HJ, Gao ZY, Xu F et al (2015) Two dimensional graphitic-phase C_3N_4 as multifunctional protecting layer for enhanced short-circuit photocurrent in ZnO based dye-sensitized solar cells. Chem Eng J 280:441
16. Xu J, Wang GX, Fan JJ, Liu BS, Cao SW, Yu JG (2015) gC_3N_4 modified TiO_2 nanosheets with enhanced photoelectric conversion efficiency in dye-sensitized solar cells. J Power Sources 274:77

17. Kim H, Lee J, Yantara N, Boix PP, Kulkarni SA, Mhaisalkar S et al (2013) High efficiency solid-state sensitized solar cell-based on submicrometer rutile TiO_2 nanorod and $CH_3NH_3PbI_3$ perovskite sensitizer. Nano Lett 13:2412
18. LiaoYL ZSM, Ma J, Sun ZH, Yin C, Zhu CL et al (2014) Tailoring the morphology of g-C_3N_4 by self-assembly towards high photocatalytic performance. ChemCatChem 6:3419
19. Ge L, Han CC (2012) Synthesis of MWNTs/gC_3N_4 composite photocatalysts with efficient visible light photocatalytic hydrogen evolution activity. Appl Catal B 117:268
20. Dai K, Lu LH, Liang CH, Liu Q, Zhu GP (2014) Heterojunction of facet coupled gC_3N_4/surface-fluorinated TiO_2 nanosheets for organic pollutants degradation under visible LED light irradiation. Appl Catal B 156:331
21. Baker DR, Kamat PV (2009) Photosensitization of TiO_2 nanostructures with CdS quantum dots: particulate versus tubular support architectures. Adv Funct Mater 19:805
22. Chang F, Zhang J, Xie YC, Chen J, Li CL, Wang J et al (2014) Fabrication, characterization, and photocatalytic performance of exfoliated gC_3N_4–TiO_2 hybrids. Appl Surf Sci 311:574
23. Wang JX, Huang J, Xie HL, Qu AL (2014) Synthesis of gC_3N_4/TiO_2 with enhanced photocatalytic activity for H_2 evolution by a simple method. Int J Hydrogen Energy 39:6354
24. Yan SC, Li ZS, Zou ZG (2009) Photodegradation performance of g-C_3N_4 fabricated by directly heating melamine. Langmuir 25:10397
25. Samanta S, Martha S, Parida K (2014) Facile synthesis of Au/g-C_3N_4 nanocomposites: an inorganic/organic hybrid plasmonic photocatalyst with enhanced hydrogen gas evolution under visible-light irradiation. ChemCatChem 6:1453
26. Li YG, Wei XL, Li HJ, Wang RR, Feng J, Yun H, Zhou AN (2015) Fabrication of inorganic–organic core-shell heterostructure: novel CdS@gC_3N_4 nanorod arrays for photoelectrochemical hydrogen evolution. RSC Adv 5:14074
27. Bai J, Li JH, Liu YB, Zhou BX, Cai WM (2010) A new glass substrate photoelectrocatalytic electrode for efficient visible-light hydrogen production: CdS sensitized TiO_2 nanotube arrays. Appl Catal B 95:408
28. Mamakhel A, Tyrsted C, Bojesen ED, Hald P, Iversen BB (2013) Direct formation of crystalline phase pure rutile TiO_2 nanostructures by a facile hydrothermal method. Cryst Growth Des 13:4730
29. Bojdys MJ, Müller JQ, Antonietti M, Thomas A (2008) Ionothermal synthesis of crystalline, condensed, graphitic carbon nitride. Chem Eur J 14:8177
30. Tan GQ, Li ZP, Yuan HY, Dan X (2014) Sorption of cadmium from aqueous solution with a highly effective sorbent-B-doped g-C_3N_4. Sep Sci Technol 49:1566
31. Su FL, Lu JW, Tian Y, Ma XB, Gong JL (2013) Branched TiO_2 nanoarrays sensitized with CdS quantum dots for highly efficient photoelectrochemical water splitting. Phys Chem Chem Phys 15:12026